Cross-linked lyotropic liquid crystal particles functionalized with antimicrobial peptides

International Journal of Pharmaceutics 627 (2022) 122215

Contents lists available at ScienceDirect

International Journal of Pharmaceutics

journal homepage: www.elsevier.com/locate/ijpharm

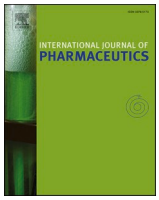

Cross-linked lyotropic liquid crystal particles functionalized with antimicrobial peptides

Edvin Blomstrand [a,b], Anand K. Rajasekharan [b], Saba Atefyekta [b], Martin Andersson [a,b,*]

[a] Department of Chemistry and Chemical Engineering, Applied Chemistry, Chalmers University of Technology, Kemigården 4, Göteborg SE-41296, Sweden
[b] Amferia AB, Astra Zeneca BioVentureHub c/o Astra Zeneca, Pepparedsleden 1, Mölndal SE-431 83, Sweden

A B S T R A C T

Antimicrobial peptides (AMPs) are promising alternatives to traditional antibiotics for addressing bacterial infections – including life-threatening antibiotic resistant infections. AMPs have a broad spectrum of antimicrobial activity and show a low probability to induce resistance. However, the poor serum stability of AMPs has limited their usage in clinical treatment. To enable improved serum stability while maintaining high antibacterial effect of AMPs, this study describes a material wherein AMPs are covalently bonded to micro-sized particles of cross-linked lyotropic liquid crystals, formed by the self-assembly of the block copolymer Pluronic F-127. The liquid crystal particles were shown to have antibacterial effect corresponding to a 4 log reduction against *Staphylococcus aureus*. The particles were structurally and chemically analyzed by small angle X-ray scattering, Fourier transform infra-red spectroscopy and Raman spectroscopy, confirming that the liquid crystal structure was maintained within the particles with the AMPs covalently bonded. The bonding to the particles gave the AMPs improved stability in serum, as they retained almost all of the antibacterial potency for 2 days compared to free AMPs, which lost all of its antibacterial potency within a day. Furthermore, insight regarding mode of action was obtained by cryogenic transmission electron microscopy, which showed the antimicrobial particles interacting with the surface of bacteria.

1. Introduction

Humankind have never had a higher life expectancy than now. Through continuous development in medicine and healthcare, a range of diseases that have been ever-present throughout history have been all but eradicated. However, microbial infections are still present and have the potential to paralyze our way of living. It is therefore evident that more work needs to be done in the field of treating and preventing microbial infections. For instance, disruption of the skin barrier, by trauma, burn or even surgical incisions, will create an opportunity for bacteria to colonize and infect our bodies (Magill et al., 2014; Zuarez-Easton, 2017; Wang et al., 2018; Neopane, 2018). Antibiotics have made wonders when it comes to treatment of these kinds of life quality impairing conditions. However, the overuse and neglect in the prescribing of antibiotics has greatly contributed to the rise of antibiotic resistant strains of bacteria that have the ability to infect us, while being completely resistant to treatment from certain types of antibiotics (Kumarasamy et al., 2010; Chambers and DeLeo, 2009; Levy and Marshall, 2004). In some cases, the resistance has also been observed towards some of the currently available last-resort antibiotics (Osei Sekyere, 2016).

There is a growing demand for alternative treatments to traditional antibiotics. For instance, a potent antibacterial agent is silver ions, which has been incorporated into wound dressings, ointment creams and as coatings on medical devices (Ong et al., 2008; Jain et al., 2009; Krishnan et al., 2020). Silver is effective and has a broad-spectrum activity, but has the drawback of needing to be eluted into the surrounding media to eradicate the bacteria (Morones et al., 2005; Kędziora et al., 2018). There is also an ongoing debate with no clear answers concerning the cytotoxicity of silver against our own cells, and the possibility of introducing resistance in bacteria (Chen and Schluesener, 2008; Muller and Merrett, 2014). Another substance that has been commonly used for its antibacterial property for centuries is honey (Gómez-Caravaca et al., 2006). While honey is interesting due to its wound healing properties and low cytotoxicity, honey's antibacterial effect is much lower than that of silver, and the concentration of honey needed is therefore questionable.

In recent years, a growing body of work has indicated the potential of antimicrobial peptides (AMPs) as a viable alternative for treating bacterial infections, with initial focus on wounds. As AMPs are an effective part of the mammalian innate immune system, they have been researched for decades on their mode-of-action and antimicrobial

* Corresponding author at: Department of Chemistry and Chemical Engineering, Applied Chemistry, Chalmers University of Technology, Kemigården 4, Göteborg SE-41296, Sweden.
E-mail address: martin.andersson@chalmers.se (M. Andersson).

https://doi.org/10.1016/j.ijpharm.2022.122215
Received 18 May 2022; Received in revised form 13 September 2022; Accepted 16 September 2022
Available online 22 September 2022

activity (Selsted et al., 1985). In brief, AMPs are short amphiphilic and positively charged peptides (Zasloff, 2002). The combination of charge and amphiphilicity give AMPs their selectivity against the negatively charged surfaces found on both gram-negative and gram-positive bacteria, as well as on some enveloped viruses and fungi (Shai, 2002; Yasin et al., 2000). This results in that AMPs can have a broad-spectrum activity while being non-toxic towards the net neutrally charged mammalian cells at effective concentrations. The main reason AMPs have not made a bigger impact in medicine is because of their low stability in biological environments such as serum, due to proteolytic degradation and inhibition of activity due to high ionic concentration and interactions with serum components (Kim et al., 2014; Nguyen et al., 2010). This stability issue is of less concern *in vivo* for the immune system, when cells like macrophages can continuously deliver a supply of AMPs at the local site of treatment, but poses a bigger challenge for the incorporation of AMPs into a potential pharmaceutical or medical device. One way of dealing with this issue is to load the AMPs into carriers in the form of nanoparticles or wound dressings to protect the AMPs until they are released (Wang, 2020; Meikle et al., 2021; Håkansson et al., 2021; Boge et al., 2019). These studies showed that AMPs can indeed be successfully loaded and protected until released which then effectively killed bacteria. Once the peptides are released, however, they still face the same issues as if they were delivered in their free form, i.e. inhibition by interaction with serum components and proteolysis by enzymes. Other methods of providing the AMPs with protection has also been studied, in which the peptides are conjugated to different materials with uses such as wound dressings and catheters (Zhu et al., 2019; Lim et al., 2015). The results show that the AMPs can maintain their antibacterial properties in a contact killing manner, meaning that if a bacterial cell makes its way to the surface of the material, they are killed.

The idea behind this study was to combine two approaches of having a fully cross-linked system with antimicrobial peptides covalently attached to the surface, not only as a macroscopic sheet or tubes for wound dressing or catheters but rather as particles that can also work in a solution. The benefits of this would be a material with high surface area, which could be used both topically on skin or in a wound as well as in a suspension that can be applied onto non-uniform or deep wounds, where a regular wound dressing or patch may be ineffective. This is achieved while providing the AMPs with protection from serum for a prolonged antibacterial effect. Previous work performed by our group has shown that covalent attachment of the synthetic AMP with the amino acid sequence RRPRPRPRPWWWW-NH_2 (derived from PRELP, net charge of +6 at a pH of 7) to the surface of a soft amphiphilic hydrogel sheet retained the antibacterial activity of the AMP in addition to increasing its proteolytic stability (Atefyekta et al., 2021; Malmsten et al., 2011). The covalent attachment was achieved by using EDC and NHS which links a carboxylic acid to a primary amine in order to form a peptide bond. The peptide bond for these material types were proven to be successful by QCM-D, zone of inhibition and leaching studies (Atefyekta et al., 2021; Atefyekta, 2019). However, the design of 3D hydrogel sheets with AMPs limits its application to surface wounds due to the fact that the bacteria need to come in physical contact with the material. Therefore, the aim of this study was to make use of the previously developed contact killing AMP-hydrogel material by formulating it into smaller discrete particles.

The particles are made out of diacrylated Pluronic F-127, a block copolymer with low cytotoxicity, which self-assembles into micelles and lyotropic liquid crystals when mixed with water and other solvents (Diniz et al., 2015; Müller et al., 2015). In this study, the concentration used (30 wt% Pluronic in 70 wt% water) corresponds to the normal micellar cubic phase (Holmqvist et al., 1997; Holmqvist et al., 1997). The particles are also of a hydrogel nature, meaning that they can have additional benefits for a wound by keeping it moist, for optimal healing conditions (Koehler et al., 2018). The usage of Pluronic F-127 in combination with AMPs has been studied before, both for drug delivery as well as antibacterial coatings (Muszanska et al., 2014; Su et al., 2019). However, the properties of Pluronic F-127 utilized in these studies are usually its thermosensitive gelling, meaning that it can be injected cold as a liquid and then turn in to a gel when heated up by the body and therefore staying in one spot to deliver drugs. Another feature is the antifouling effect Pluronic F-127 as a coating, functioning as a PEGylated surface. This study further expands the usage of Pluronic F-127 as a material base for a new combination of antimicrobial peptide system. By the covalent binding of AMPs and Pluronics, a material system that is effective and stable is formed, a feature that has not been achieved previously using Pluronic F-127 polymers.

2. Materials and methods

2.1. Materials

Diacrylated Pluronic F-127, poly(ethylene oxide)$_{100}$-poly(propylene oxide)$_{70}$-poly(ethylene oxide)$_{100}$, with a molecular weight of 12 600 g/mol and with a guaranteed purity of ≥95 % (abbreviated here as DA-PF127) and the antimicrobial peptide (AMP) RRPRPRPRPWWWW-NH_2 (C-terminus amidated and *N*-terminus left unchanged), with a molecular weight of 1930 g/mol and with a guaranteed purity of ≥90 % was received as a gift from Amferia AB. *N*-hydroxysuccinimide (NHS) and 1-ethyl-3-(3-dimethylaminopropyl)carbodiimide (EDC) were purchased from Fisher Scientific. MES buffer, NaOH, 2-hydroxy-4′-(2-hydroxyethoxy)-2-methylpropiophenone, tryptic soy broth, brain heart infusion agar, phosphate buffered saline (PBS) and Mueller Hinton broth were purchased from Sigma Aldrich.

2.2. Preparation of AMP functionalized lyotropic liquid crystal particles (antimicrobial particles)

Lyotropic liquid crystal particle samples were prepared through the following steps – 30 wt% DA-PF127 and 70 wt% Milli-Q H_2O was manually mixed with a spatula. The photoinitiator, 2-hydroxy-4′-(2-hydroxyethoxy)-2-methylpropiophenone was added to the solution at a concentration of 0.5 wt% of the dry DA-PF127 powder. The solution was placed at 4 °C for at least 48 h for the gel to transform into a liquid. This liquid was then used to cast sheets of 10x10 cm with approximately 1 mm thickness, that set into shape at room temperature. The sheets were then cross-linked by exposure to UV-light for 3 min, resulting in an approximate dose of 0.9 J/cm^2. The UV-source was UVP Crosslinker; CL-3000 M from Analytic Jena ($\lambda = 302$ nm).

The cross-linked hydrogel sheets were rinsed in a water bath constantly stirring for at least 2 days with a change of water twice a day to remove any non-cross-linked polymer and to completely swell the hydrogels. The hydrogel sheets were then grounded into course granulates using an electric coffee grinder. The granules were then further reduced in size using an ultra-turrax with water as media (T-18 digital ultra-turrax from IKA) for 15 min at 15,000 rpm. This was followed by sonication of the particles for 3 min using a Sonics Vibra-cell VC 505 with a 13 mm probe running at 40 % of full power with pulse mode: 20 s on, 20 s off with a combined operating time of 4 min. The dispersion could then be subjected to filtration in order to separate different size distributions as suitable for the application/analysis.

For AMP functionalization of the particles the following procedure was used. Particles were suction filtered using a filter paper with a pore size of 6 μm, the filter cake of particles that did not go through the filter paper, giving a size of >6 μm, were collected, weighed, and placed in falcon tubes. For each gram of particles, 5 ml of MES buffer (0.5 M, pH adjusted to ~6 with NaOH) containing 2 mg/ml of EDC and 2 mg/ml of NHS was added (EDC and NHS was added to the MES buffer just prior to usage). The dispersion was left on stirring for 30 min. The particles were then suction filtrated again, washed thrice with water and placed back into a falcon tube. For each gram of particles (swollen weight), 5 ml of AMP-solution (400 μM in PBS, forth called - activation solution) was

added to the tube. The dispersion was stirred for 2 h, suction filtered, washed thrice in water, and finally weighed into a falcon tube. The activation solution and the washing solutions were subjected to UV–vis analysis to determine the amount of AMP that was taken up by the particles. This was performed using the cuvette reader of a Multiskan GO from Thermo Scientific. The absorbance was read at 280 nm, which correlates to the absorbance caused by the tryptophan amino acids of the peptide. The concentration was determined using a standard curve. By measuring the stock solution of the AMPs, the amount of AMP that had been taken up by the particles was determined. To analyze the mass lost due to the filtration, freshly prepared particles were suction filtrated using a 6 μm filter that was weighed before the filtration. The filter and retained particles were placed at 50 °C until dry, and the filtrate that ran through the filter was collected in a pre-weighed petri dish and placed at 50 °C until all the water had evaporated. By weighing the petri dish and the filter plus particles after drying the retained mass could be measured.

For certain experiments as detailed in the results section, the particles were freeze-dried. Freeze-drying was chosen as a drying method to retain the lyotropic liquid crystal structure of the particles and allow for quick rehydration when necessary. The particles were first frozen inside an Erlenmeyer flask, at −20 °C. The frozen flask was then lowered in liquid nitrogen prior to being introduced into the freeze-dryer. The freeze-dryer (CoolSafe from Scanvac) was run for 24 h per 20 g of fully swollen particles.

2.3. Material characterization

2.3.1. Dynamic light scattering

The size distribution of the particles was measured using dynamic light scattering (DLS). The non-filtered particle solution, containing all sizes was analyzed using a Mastersizer MicroPlus from Malvern. The dispersion was added until an accepted signal intensity was detected by the instrument. Particles that had gone through a filter paper (≤6 μm) were analyzed by a N4 plus from Beckman Coulter. The dispersion was analyzed directly after filtration and sonication without any further dilutions and each sample was analyzed for three consecutive runs lasting 60 sec each.

2.3.2. Small-angle X-ray scattering

Small-angle X-ray scattering (SAXS) measurements were performed with a Mat:Nordic from SAXLABS/Xenocs. The samples of interest were exposed to the X-ray beam for 5 min and the data was collected over a q-range of 0.0122–0.68 $Å^{-1}$ with the detector at a distance of 477 mm from the samples. The following samples were evaluated – (a) Freeze-dried particles with and without the AMP functionalization, (b) pieces of freshly cross-linked hydrogels without any functionalization, and (c) fully swollen control particles. The samples were measured using an ambient holder where they were placed in between two pieces of tape (Scotch magic tape from 3 M). As the tape does not form an ideal seal, drying of the swollen samples is a potential risk. The pure tape was also measured, and its scattering signal was removed as background.

2.3.3. Raman and Fourier transform infrared spectroscopy

Freeze-dried control particles, antimicrobial particles, pure DA-PF127 powder, and pure AMP powder were analyzed by Raman and Fourier transform infrared (FTIR) spectroscopy. For Raman, each sample was measured three times at two different locations, using an alpha300 R from WITec with a 50X NA 0.75 objective, 532 nm laser and an intensity of 3.5 mW, and using 1 sec integration time × 10 for each run. The FTIR spectra were determined using a Vertex70V from Bruker with an attenuated total reflection. Each FTIR spectrum was compiled from 64 scans per sample.

2.4. In vitro assays

2.4.1. Cytotoxicity determination

The potential cytotoxicity was evaluated by an MTT assay. Antimicrobial particles were prepared as described earlier, and control particles without any AMP functionalization was also evaluated in order to determine if the potential cytotoxicity is coming from the inclusion of AMPs or not. The cells used were from the cell line L929 (fibroblasts from mouse) from Sigma Aldrich, and the cell media used was Gibco™ DMEM/F-12, HEPES, no phenol red, with L-Glutamine added. This was supplemented with 10 % FBS and Gentamicin (10 μg/ml) and Amphotericin B (0.25 μg/ml). The swollen particles were weighed into Eppendorf tubes to which full media was added as extraction vehicle. The particle concentration was determined by following the ISO 10993–12 for '*irregularly shaped porous devices (low-density materials)*' which suggests an extraction ratio of 0.1 g/ml. This was placed in the humidified incubator at 37 °C and 5 % CO_2 for 3 days with occasional agitation. Full media for the negative control were also placed in Eppendorf tubes in the incubator for 3 days to eliminate the incubation time as a factor. After extraction, the media was syringe filtered to filter out the particles and the extracts were stored at 4 °C until usage.

The cells were cultured until confluent, where they were treated with trypsin-EDTA, centrifuged, and finally resuspended in full media. The cell concentration was measured by using a Bürker counting chamber. 200 μl of the different extraction medias, negative control, and positive control (1 % Triton X-100 in full media) were added to the wells of two 96 well plates (one for each time point). To each well, 10, 000 cells were added, and uniformity was observed by an inverted microscope. The plates were placed in the incubator for either 24 or 48 h. After the set time, the solutions were discarded, and 100 μl of full media was added to each well, included three blanks (no cells). To each well, 10 μl of the 5 mg/ml MTT solution (from The Cell Proliferation Kit I (MTT) by Roche) was added and placed in the incubator for 4 h. Thereafter, 100 μl of 10 % SDS in 0.01 M HCl was added to each well to solubilize the formazan that the alive cells have converted the MTT into. The plates were placed back into the incubator overnight and the absorbance of each well was then measured at 570 nm by using a Multiskan GO from Thermo Scientific. The viability was determined by: $(A_{Sample} - A_{Blank})/(A_{Negative\ control} - A_{Blank})$.

2.4.2. Hemolysis study

Defibrinated horse blood was acquired from Fisher Scientific, stored at 4 °C and used within 4 weeks. Blood was transferred into 15 ml falcon tubes and centrifuged at 1000 × g for 10 min at 4 °C. The supernatant was discarded, and the red blood cells were resuspended in PBS and centrifuged down again, and the supernatant discarded. This washing was repeated for a total of 4 times. The red blood cells were finally resuspended in PBS at a concentration of 2 % (v/v). Antimicrobial particles were prepared as previously described and prepared in a dilution series starting at 50 mg/ml (dry weight) and diluted to 1:512 by factors of 2, each tube containing particles in 100 μl PBS. A dilution series of pure AMP in PBS (100 μl) was also prepared with the highest concentration being 200 μM and diluted by a factor of 2 until 1:512 (all the concentrations are for the final solution). Negative controls using just PBS and positive controls using 0.1 % (v/v) Triton X-100 were also used. 100 μl of the 2 % (v/v) blood solution was added to each tube, which were all gently vortexed and placed in an incubator at 37 °C for 1 h. The tubes were gently vortexed 30 min into incubation as well as after the 1 h was up. The Eppendorf tubes were finally centrifuged again and 100 μl of the supernatants were transferred to a 96 well plate and the absorbance at 540 nm was measured using a Multiskan GO from Thermo Scientific. The hemolysis was determined as: $(A_{Sample} - A_{Negative\ control})/(A_{Positive\ control} - A_{Negative\ control})$.

2.4.3. Microorganisms

The microorganisms used in this study were *Staphylococcus aureus*

(CCUG 10778), *S. aureus* MRSA (CCUG 41586), *S. aureus* MRSA (CCUG 74135) *Escherichia coli* (CCUG 29300T), *Pseudomonas aeruginosa* (CCUG 56489) and *Staphylococcus epidermidis* (CCUG 31568). The bacteria were stored at −80 °C for long term storage and were streaked and cultivated on brain heart infusion (BHI) agar plates in order to acquire single colonies. The plates with colonies were stored at 4 °C for easy access and were used within three weeks.

2.4.4. Minimum inhibitory concentration assay

A colony of either *S. aureus,* MRSA 41586, MRSA 74586, *S. epidermidis, E. coli* or *P. aeruginosa* was inoculated into Mueller Hinton broth (MH-broth) and incubated at 37 °C until they had grown to approximately 10^9 colony forming units (CFU)/ml (mid-log growth), determined by measuring the optical density. The samples analyzed in this test were pure AMP dissolved in MH-broth and antimicrobial particles (>6 μm) dispersed in MH-broth. 500 μl of MH-broth was added to the wells of a 24 well plate (except for the first dilution, 1:1). 500 μl of the test solutions were then added to the 1:1 and 1:2 dilutions, 500 μl of the 1:2 dilution was then added to the 1:4 dilution etc. until a dilution of 1:512 was obtained. The bacteria were then diluted to 10^6 CFU/ml of which 500 μl was added to each well for a final concentration of 5 * 10^5 CFU/ml per well. A negative control was used containing only media and bacteria and also a blank containing only media. The plates were incubated overnight at 37 °C, and the morning after (roughly 18 h later) the wells with the lowest concentration of test solution in which no growth was observed was noted down as the minimum inhibitory concentration (MIC).

2.4.5. Agar plate model

A colony of *S. aureus* was inoculated in tryptic soy broth (TSB) and cultivated at 37 °C until a concentration of approximately 10^9 CFU/ml was reached, checked by measuring optical density. The solution was diluted to a concentration of 10^8 CFU/ml. A cotton swab was then dipped in the solution and used to streak BHI agar plates. The plates were left on the bench until no liquid from the bacteria solution was observed on the agar. 200 mg of particles dispersed in 200 μl of PBS was gently spread on top of the agar plates until a homogenous spread without any major gaps was obtained. Each plate was spread with one AMP-functionalized sample and one non functionalized sample (control). The plates were incubated overnight at 37 °C. The following day, the bacterial lawn was observed on the plates, a homogenous lawn with full coverage (on the non-treated parts) was necessary for the assay to be deemed valid. Images were taken of the plates and a 4 mm Ø biopsy punch (including both agar and particles) was taken from the middle of each spread and placed into Eppendorf tubes containing 1 ml of PBS. The tubes were vortexed for 10 sec and put on a shaker for 5 min. Dilution series by factors of 10 were performed. Two drops of 10 μl were taken from each dilution and placed on BHI-agar plates and incubated at 37 °C overnight. The following morning the drops of the dilutions containing 5–50 colonies were counted and the corresponding CFU/ml of the Eppendorf tubes were calculated.

2.4.6. Serum stability

A colony of *S. epidermidis* was inoculated in TSB and cultivated at 37 °C until it had reached mid log growth and a concentration of approximately 10^9 CFU/ml (determined by optical density). The bacteria was then diluted in PBS to a concentration of approximately 10^8 CFU/ml. Free AMP was prepared in PBS and 720 μl of the AMP solution was added to Eppendorf tubes in concentrations so that it forms 40 μM and 60 μM in 1 ml. In other Eppendorf tubes 60 mg and 90 mg (dry weight) of antimicrobial particles were weighed and 720 μl of PBS was added to these tubes. Negative controls containing only 720 μl of PBS were also used. For the 'without serum' samples, 180 μl of PBS was added to each tube, and for the other samples, 180 μl of full human male serum was added and either evaluated immediately (called 'with serum'), left in incubator for 1 day, or left in incubator for 2 days. At the corresponding evaluation time, 100 μl of the 10^8 CFU/ml bacterial solution was added to each tube (this means that the samples will incubate in 20 % serum for 1 or 2 days, and 18 % serum when bacteria is present). The tubes were then vortexed for 5 sec and placed at 37 °C for 10 min. After the 10 min, the tubes were again vortexed for 5 sec and serial diluted by factors of 10. Two drops of 10 μl were taken from each dilution and placed on BHI-agar plates and incubated overnight. The following morning the drops of the dilutions containing 5–50 colonies were counted and the corresponding CFU/ml of the Eppendorf tubes were calculated.

2.4.7. Cryogenic transmission electron microscopy

A particle dispersion was filtered through a 6 μm suction filter and a 0.2 μm syringe filter in order to obtain sets of sub-micron sized particles. Half of the solution was functionalized by adding AMP and EDC/NHS for a final concentration of 100 μM and 1 mg/ml respectively. The solution was left to react for 2 h followed by centrifugation at 12, 000 × g (using a Megafuge 16R from Thermo Scientific) for 80 min, in order to concentrate the particles and remove excess AMP from the solution. The particles were redispersed in PBS and sonicated. The samples were then delivered to Umeå Core Facility for Electron Microscopy (UCEM), Umeå University, Sweden where sample preparation and measurements were performed. A culture of *S. aureus* (CCUG 10778) was placed in TSB and cultivated for 4 h and centrifuged to a pellet at 3000 × g for 3 min. The supernatant was then removed, and the bacteria was resuspended in the particle solutions to an OD of 6. The bacteria and particles were incubated for 1 h and was then plunge-frozen in liquid ethane onto a carbon-coated grid. The grids were then kept in liquid nitrogen and placed into the FEI Titan Krios TEM where the samples were maintained at cryogenic conditions throughout the measurements.

3. Results

3.1. Particle preparation

Fig. 1 show the different steps of the particle synthesis, from the first mixture of the polymer, photo initiator and water (Fig. 1a) to the freeze-dried particles (Fig. 1f). DA-PF127 mixed with H_2O becomes a liquid at 4 °C and turns into a very viscous gel at room temperature (Fig. 1b & c). The gels were cross-linked into the sheets seen in Fig. 1d which in turn were processed into the particle granules as seen in Fig. 1e. By weighing the particles before and after freeze-drying (Fig. 1f) it showed that the fully swollen particles contained around 90 % water by weight. UV-measurements showed that the particles (Fig. 1e) were functionalized with 3.3 mg of AMP per 100 mg of dry particles. The corresponding functionalization of the hydrogel shown in Fig. 1d was 1 mg per 100 mg of dry hydrogel.

3.2. Dynamic light scattering

The size distribution obtained for the whole range from the Mastersizer can be found in the supplementary information (Fig. S1). It shows that the majority of the mass can be found in particles with sizes between 100 and 500 μm. When the population is weighed on the number of particles with a certain size however, it was clear that a majority of the particles have a size of 2–30 μm.

When filtered through a 6 μm filter, the retained weight of freshly made particles (>6 μm) was measured to be roughly 99.8 wt% and the weight of particles that went through the filter (<6 μm) was roughly 0.2 wt%. The size distribution of the particles that did pass through the 6 μm filter can be seen in Fig. 2. Fig. 2a shows the measured DLS intensity of control particles that have two clear size distributions, 20–60 nm, and 90–350 nm. Three consecutive measurements were run for 60 sec each, which showed very similar distributions over time. Fig. 2b shows the measured DLS intensity of the filtrated antimicrobial particles. The distributions changed somewhat over the course of the three consecutive

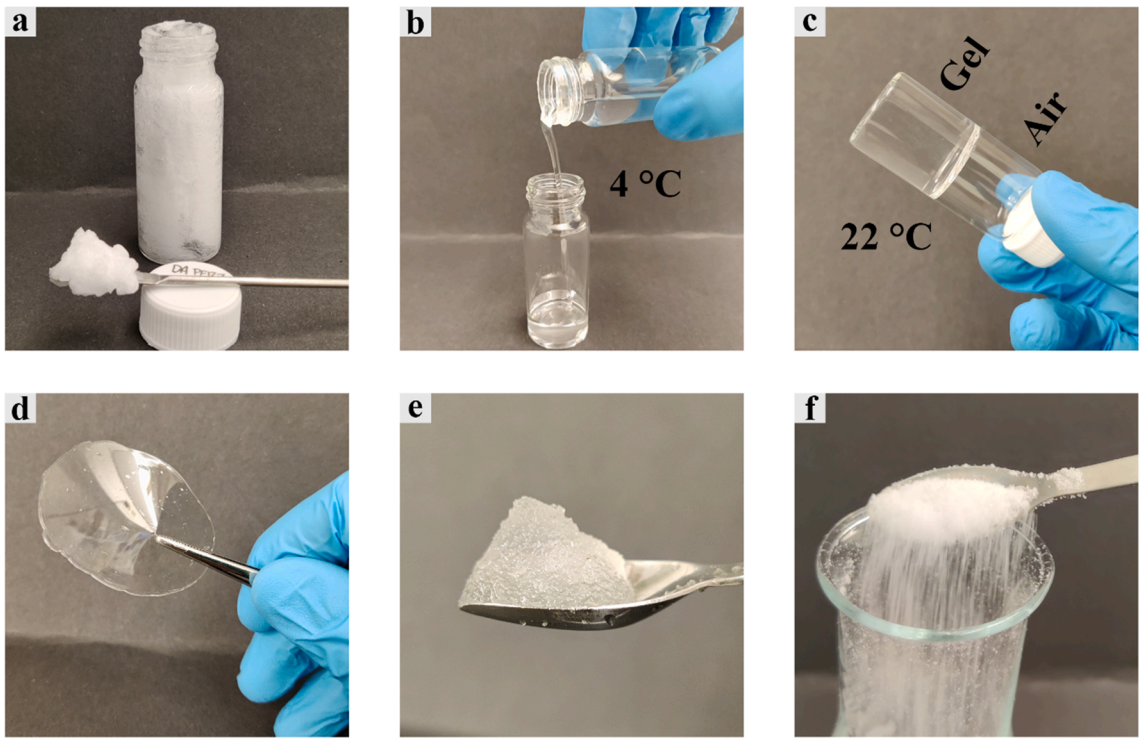

Fig. 1. Images taken of the different steps of the particle formation process. (a) The gel mixture directly after mixing. (b) The gel solution at 4 °C after being stored at 4 °C for 72 h. (c) The same solution after it has equilibrated to room temperature. (d) The hydrogel after it has been cross-linked between glass slides. (e) The particles made by grinding, ultra-turraxing and sonicating hydrogels shown in (d). (f) The particles after they have been freeze-dried.

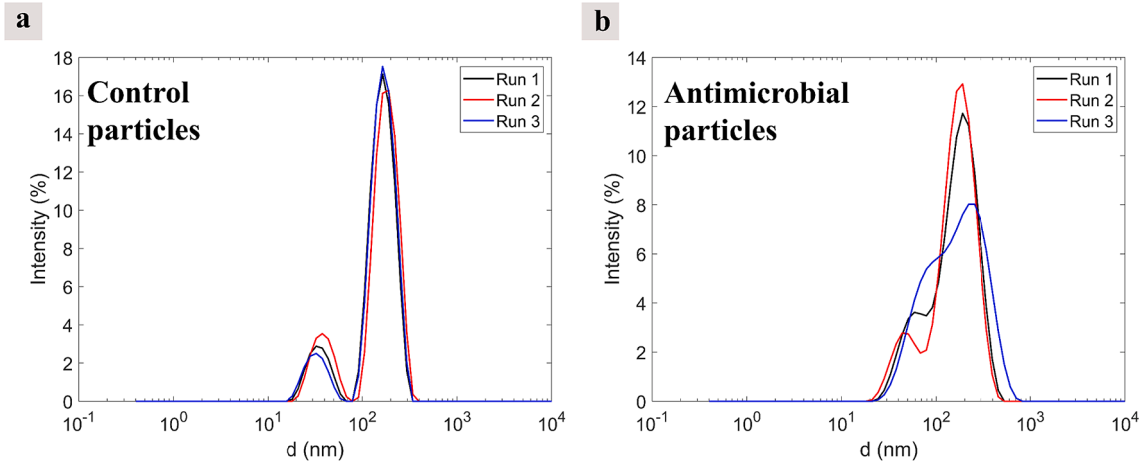

Fig. 2. Size distribution measured by DLS of the filtrated (<6 μm) particles. (a) The size distribution of non-functionalized control particles over three consecutive 60 sec runs. (b) The size distribution of the antimicrobial particles over three consecutive 60 sec runs.

runs but showed sizes between 20 and 700 nm.

3.3. Small angle X-ray scattering

The results from the SAXS measurements can be seen in Fig. 3. A clear diffraction peak was seen in all the measured samples indicating that an ordered nanostructure was present in all samples. A minor peak shift of roughly 0.005 $Å^{-1}$ to higher q values was observed by the swollen particles compared to the X-ray scattering data of the dried particles. No secondary peaks were found in any of the samples.

3.4. Fourier transform infrared and Raman spectroscopy

The FTIR spectra are presented in Fig. 4. The full spectra can be seen in Fig. 4a and a zoomed in section between the wavenumbers 1520–1820 cm^{-1} can be seen in Fig. 4b, since this is where the C═O stretch is found. The most noticeable difference between the Pluronic-containing systems is a slight peak shift and broadening from 1725 cm^{-1} for the DA-PF127 to 1735 cm^{-1} for the particles. Furthermore, there is a broad peak in both of the AMP containing systems around 1650 cm^{-1}. The most likely molecular groups giving rise to these peaks can be found in Table 1.

The Raman spectra are presented in Fig. 5. By comparing the different Pluronic-containing systems differences were found. First, two

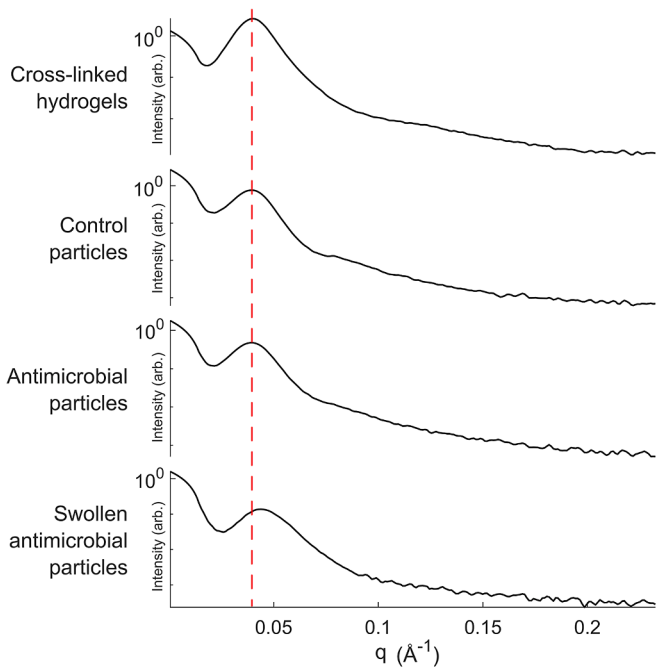

Fig. 3. SAXS diffractograms of cross-linked hydrogels (not swollen), freeze-dried control particles, freeze-dried antimicrobial particles, and fully swollen control particles. All samples were measured in between tape, which has been removed as a background from the other samples.

small peaks at ~1635 cm^{-1} and ~1730 cm^{-1} were seen in the DA-PF127 sample that were not evident in the particle samples. These two peaks are in the C═C region, which correlates well to the vinyl group at the end of the acrylate groups. Between the antimicrobial particles and control particles there were three clear new peaks in the antimicrobial

Table 1
The molecular structure of the groups of interest and their corresponding frequency ranges in which they are found.

Name	Frequency range (cm^{-1})	Molecular structure
IR		
Amide	1690–1680	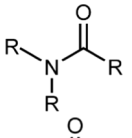
Conjugated ester	1730–1715	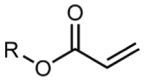
Ester	1750–1735	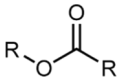
Carboxylic acid	1760	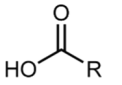
Raman		
Vinyl	1600–1700 (C═C bonds)	
Indole	756 1010	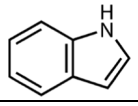

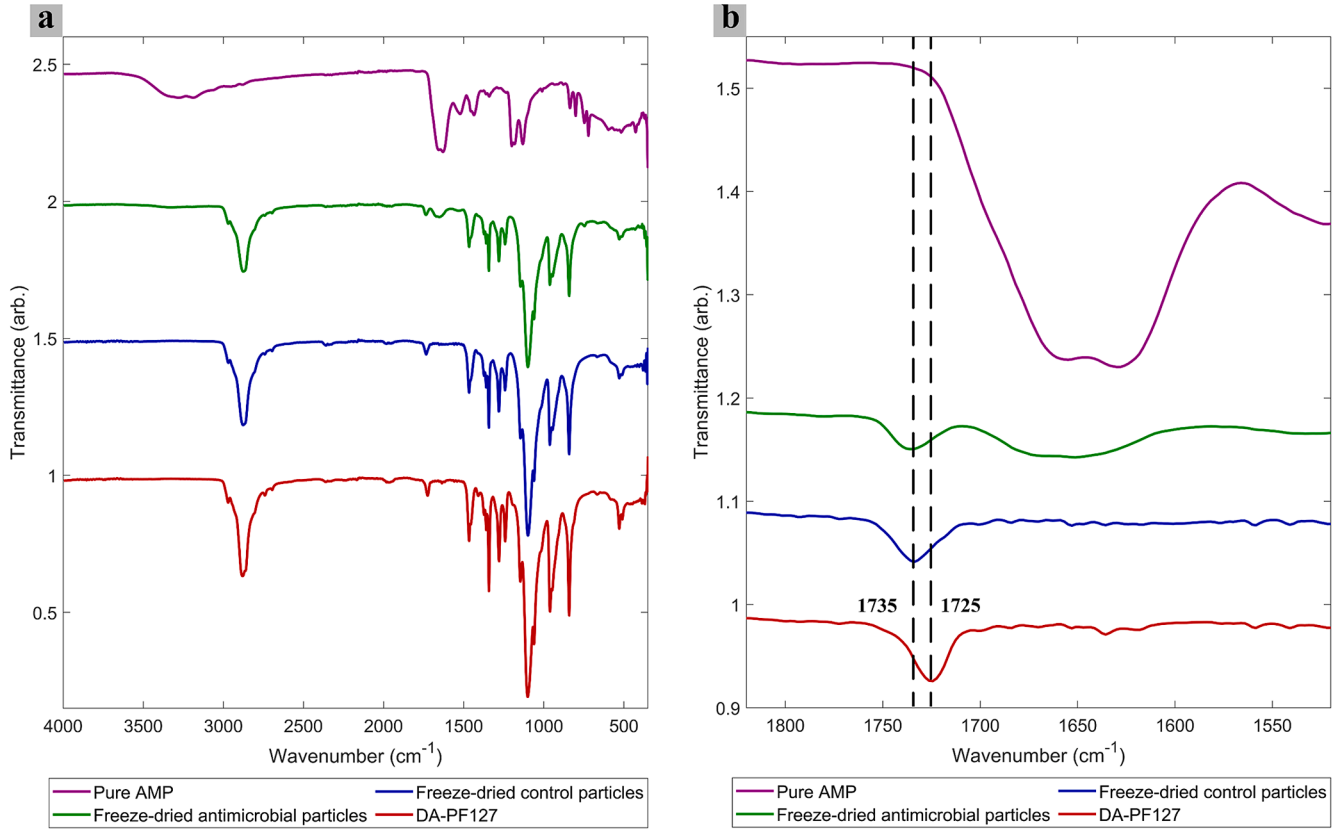

Fig. 4. FTIR spectra of pure AMP (purple), antimicrobial particles (green), control particles (blue) and the DA-PF127 (red). a) The full spectra. b) A zoomed in section of wavenumbers between 1520 and 1820 cm^{-1}. Two lines have been drawn in b) where the left one is drawn at 1735 cm^{-1} and the right one is drawn at 1725 cm^{-1}. (For interpretation of the references to color in this figure legend, the reader is referred to the web version of this article.)

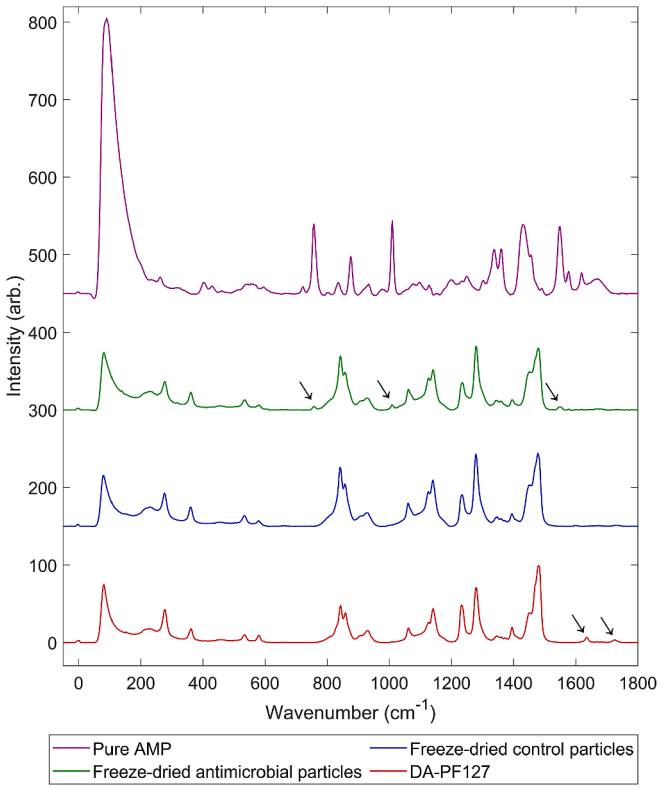

Fig. 5. The measured Raman spectra for the pure AMP (purple), antimicrobial particles (green), control particles (blue), and DA-PF127 (red). The black arrows indicate specific signals that are reaction specific. (For interpretation of the references to color in this figure legend, the reader is referred to the web version of this article.)

particles that were not present in the control particles. The peaks can be seen at 750 cm^{-1}, 1010 cm^{-1} and 1550 cm^{-1}. Three narrow and strong peaks were also found at these wavenumbers in the pure AMP. Two of them likely correlate to the indole groups of the tryptophan amino acids (750 and 1010 cm^{-1}) (Zhu et al., 2011). These functional groups can be seen in Table 1.

3.5. Cytotoxicity and hemolysis

The cell viability of the extracts cultivated with L929 mouse fibroblasts for 1 and 2 days can be observed in Fig. 6. The extracts from the control particles showed a slight reduction in viability to around 90 % for 1 day and 92 % for 2 days. The incorporation of AMPs for the antimicrobial particles reduced the viability slightly more to 81 % for 1 day and 74 % for 2 days. All data was above the threshold of 70 % viability recommended by the ISO standard as a cut-off for signs of cytotoxicity. The morphology of the cells and the positive control behaved as expected, and the study was concluded to be valid.

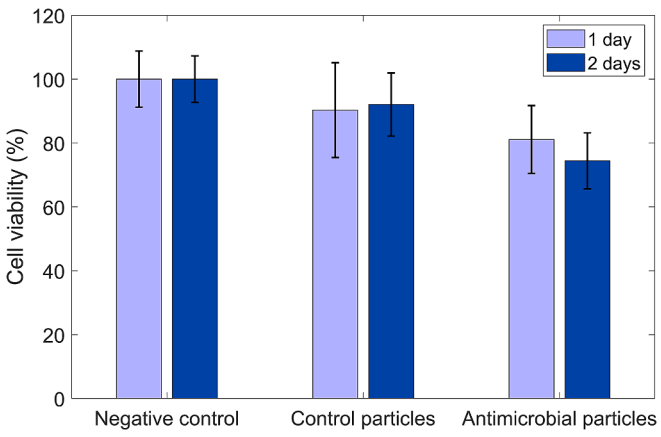

Fig. 6. The cell viability of L929 mouse fibroblasts measured by a MTT test against extracts from control and antimicrobial particles cultivated for 1 and 2 days. N = 9 and the error bars show the standard deviation.

The results from the hemolysis study of red blood cells from horse blood are shown in Fig. 7. The free AMP demonstrated a concentration dependence to hemolysis, with almost 100 % hemolysis at 200 μM which decreased at lower AMP concentrations. The antimicrobial particles did not follow the same trend but instead had a very similar hemolysis result between 5 and 10 % regardless of concentration.

3.6. Minimum inhibitory concentration assay

The MIC values are presented in Table 2. Very similar, and quite low, MIC values were observed against all *Staphylococci* and *E. coli*, including the MRSA strains. This was the case both for the free AMPs and the antimicrobial particles. The antibacterial effect was less potent towards *P. aeruginosa,* and a higher concentration was necessary to inhibit proliferation for both the free AMPs and the particles. Furthermore, when evaluated in terms of AMP present in the particles and comparing it to the free AMP (μg/ml of AMP), it was evident that 10–30 times more of the AMP was necessary to achieve inhibition for all bacteria.

3.7. Agar plate model

A representative image of the agar plate after *S. aureus* was cultivated overnight on the plates is shown in Fig. 8a. The left image shows the spread of control particles and to the right, the spread of antimicrobial particles. The color of the plate in the presence of the control spread changed into beige, indicating that bacteria was present and thriving. The presence of antimicrobial particles resulted in a transparent agar beneath, indicating fewer bacteria. This is supported by the counted CFU from the middle of the spreads, shown in Fig. 8b. No obvious zone of inhibition was observed around any of the particle spreads, indicating that AMPs had not leached out in concentrations high enough to inhibit bacterial growth. The control particle spread had a mean concentration of $2.5 \pm 1.0 * 10^8$ CFU/ml and the antimicrobial particle spread had a mean concentration of $1.7 \pm 2.5 * 10^4$ CFU/ml. This corresponds to a surface concentration of $1.98 \pm 0.79 * 10^9$ CFU/cm^2 for the control particles and $1.35 \pm 1.98 * 10^5$ CFU/cm^2 for the antimicrobial particles.

3.8. Serum stability

The findings from the serum stability test are presented in Fig. 9. The CFU/ml of *S. epidermidis* for the different concentrations of free AMP and antimicrobial particles are shown when cultured without serum (Fig. 9a), with serum (Fig. 9b), after 1 day in serum (Fig. 9c), and after 2 days in serum (Fig. 9d). The PBS control were consistent in all set ups. The free AMP samples showed a very strong antibacterial effect without serum while the antimicrobial particles showed less of an effect but still significant. With the serum present the free AMPs lost quite a bit of their activity and showed the same activity as the antimicrobial particles. For both 1 and 2 days in serum the free AMP no longer had any antibacterial effect as the CFU was the same as the PBS control. The Antibacterial particles however, retained almost all of their antibacterial effect after 1 and 2 days in serum.

3.9. Cryogenic transmission electron microscopy

Fig. 10 show cryogenic transmission electron microscopy (cryo-EM) images taken of *S. aureus* that has been cultivated for 1 h with filtrated antimicrobial particles and then plunge-frozen in liquid ethane. This was done to enable imaging of potential interaction between the bacteria

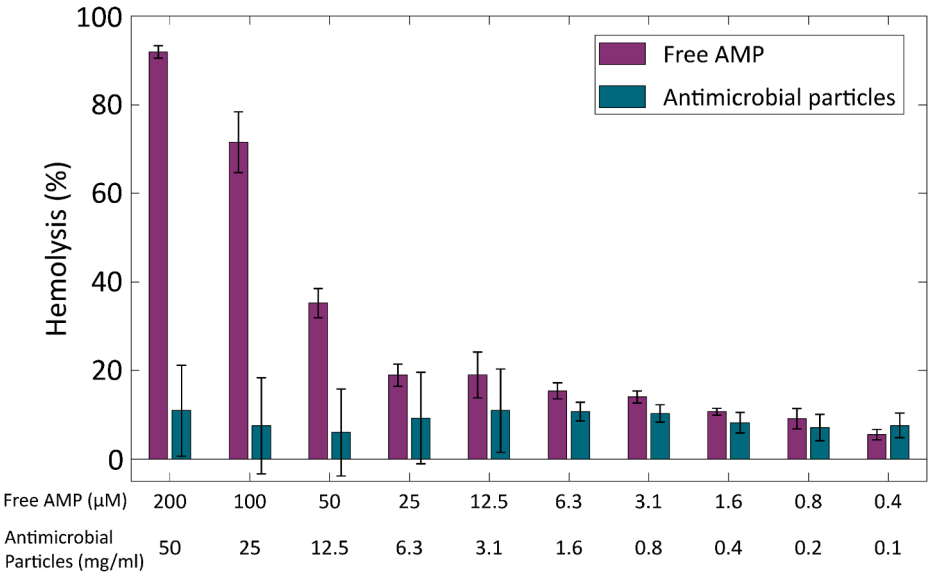

Fig. 7. Hemolysis of red blood cells from horse blood. The susbstances tested were free AMPs and antimicrobial particles. The results are the average from three independent experiments. (For interpretation of the references to color in this figure legend, the reader is referred to the web version of this article.)

Table 2
MIC values against six bacterial strains. The tests were performed in three independent experiments and if different concentrations were observed at different separate runs, an interval of concentrations is presented.

	Free AMP		Antimicrobial particles	
	μM	μg/ml of AMP	mg/ml	μg/ml of AMP
S. aureus	1.6	3	0.8–3.1	26–103
S. aureus MRSA, 41586	1.6–3.1	3–6	0.4–0.8	13–26
S. aureus MRSA, 74135	1.6–6.2	3–12	0.4–1.6	13–52
S. epidermidis	3.1	6	0.8–1.6	26—52
E. coli	1.6–3.1	3–6	1.6–3.1	52–103
P. aeruginosa	6.3–12.5	12–24	12.5–25	413–825

and the particles that take place in the natural environment as no fixation or staining of the samples is carried out. In Fig. 10a and b a particle with a diameter of roughly 250 nm can be observed in direct contact with a bacterial cell. It also appears as if some deformation of the particle is seen as well as some irregularities in the cell wall/membrane. Fig. 10c and d show a particle with roughly 180 nm across (the spherical section) that appear to be highly deformed and squeezed in between two bacterial cells.

4. Discussion

This study presented a method to produce fully cross-linked antimicrobial lyotropic liquid crystal particles with covalently bonded antimicrobial peptides. Through a top-down size reduction approach to make the particles, i.e. blending, ultra-turraxing and sonicating, a broad size distribution was obtained. If a specific size is desired, it is therefore

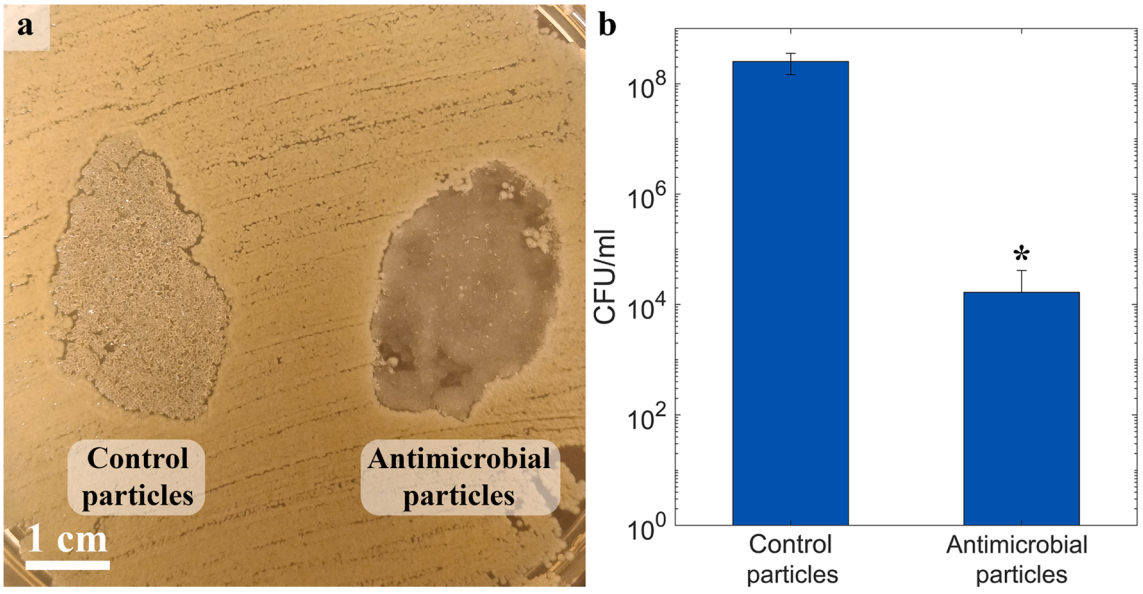

Fig. 8. (a) An image of the top of an agar plate cultivated over night with S. aureus. Control particles are spread on the left and antimicrobial particles are spread on the right. (b) The measured CFU/ml of biopsy punches taken from the middle of the spreads shown in a. N = 9 and the error bars show the standard deviation. The '*' indicates a statistically significant difference compared to the control with $p < 0.05$.

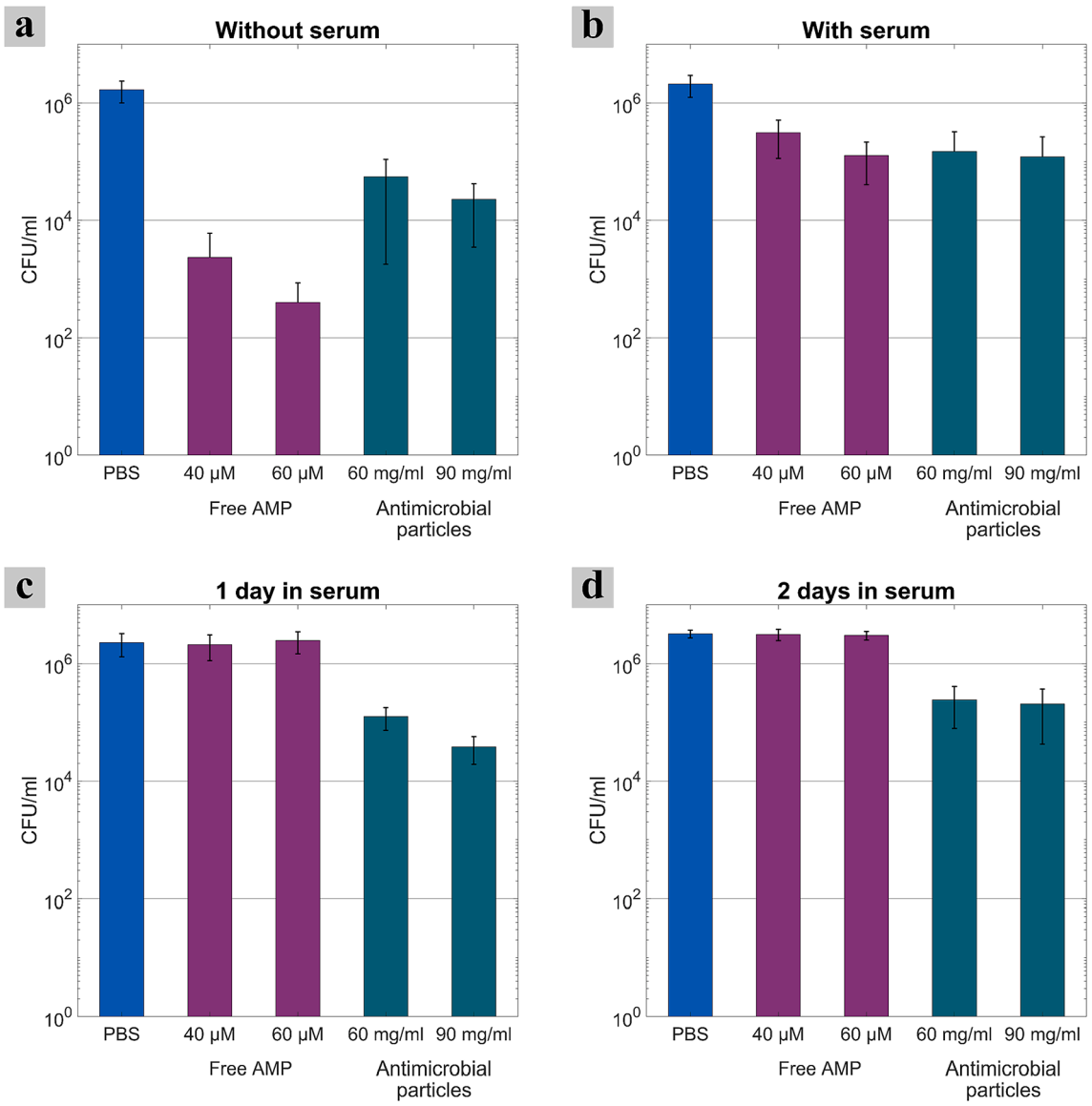

Fig. 9. The bacterial concentration of *S. epidermidis* measured in PBS, for two different free AMP concentrations, and two antibacterial particle concentrations, cultivated with bacteria for 10 min. (a) Cultivation without serum present. (b) Cultivation with serum present. (c) Cultivation after 1 day in serum. (d) Cultivation after 2 days in serum. N = 6, error bars are the standard deviation.

necessary to post-process the particles with either a syringe filter or by suction filtration. The size distribution of the smallest of these particles are shown in Fig. 2, although these particles are not used in most of the antibacterial tests due to the AMP attachment protocol, they can still provide a lot of information regarding the mechanisms at play. From Fig. 2 it is evident that the attachment of the AMPs to the particles influences the size distribution, at least for these smaller particles that had been filtered through a 6 µm filter. The distribution of the antimicrobial particles is broader, and the consecutive runs showed that it was not stable between measurement cycles. This could be attributed to the dynamic balance between electrostatic repulsions and hydrophobic interactions between the AMP-functionalized particles. The hydrophobic effect would work to bring particles together, while the positive charge of the AMPs would work to keep the particles separate, but more rigorous experiments are needed to study it further. Furthermore, the two separate peaks found in Fig. 2a and to some extent also in Fig. 2b suggests a bimodal distribution. A possible explanation for this is found in the micellar cubic structure of the particles. It is possible that single cross-linked micelles may detach from these networks of packed micelles which will then show up at a different size than the rest of the particles. This hypothesis fits well with the fact that Pluronic F-127 micelles have a size of roughly 25 nm, which are slightly bigger with the incorporation of the end groups used in this study (Pragatheeswaran and Chen, 2013). A bimodal distribution is a common feature for the case of cubosomes (non-cross-linked), where the smaller size distribution represents singular vesicles and the larger size distribution represents the cubosome particles (Angelov et al., 2012; Zerkoune et al., 2016). It can therefore be speculated that the observed smaller distribution is cross-linked micelles that have been stripped away from the micellar cubic structure and that the bigger distribution is larger fractions of interconnected micelles from the micellar cubic structure.

The SAXS measurements (Fig. 3) showed that an ordered structure was present within the particles which was unaffected throughout the manufacturing process. The position of the diffraction patterns in all the diffractograms indicate the presence of micellar cubic LLC structure in the particles, specifically matching the [1 1 1] plane (Holmqvist et al., 1997; Holmqvist et al., 1997). No noticeable size difference was observed between the freshly cross-linked hydrogel and the freeze-dried particles with or without the AMPs, indicating that the AMP functionalization does not have a major impact on the size of the LLCs. A number

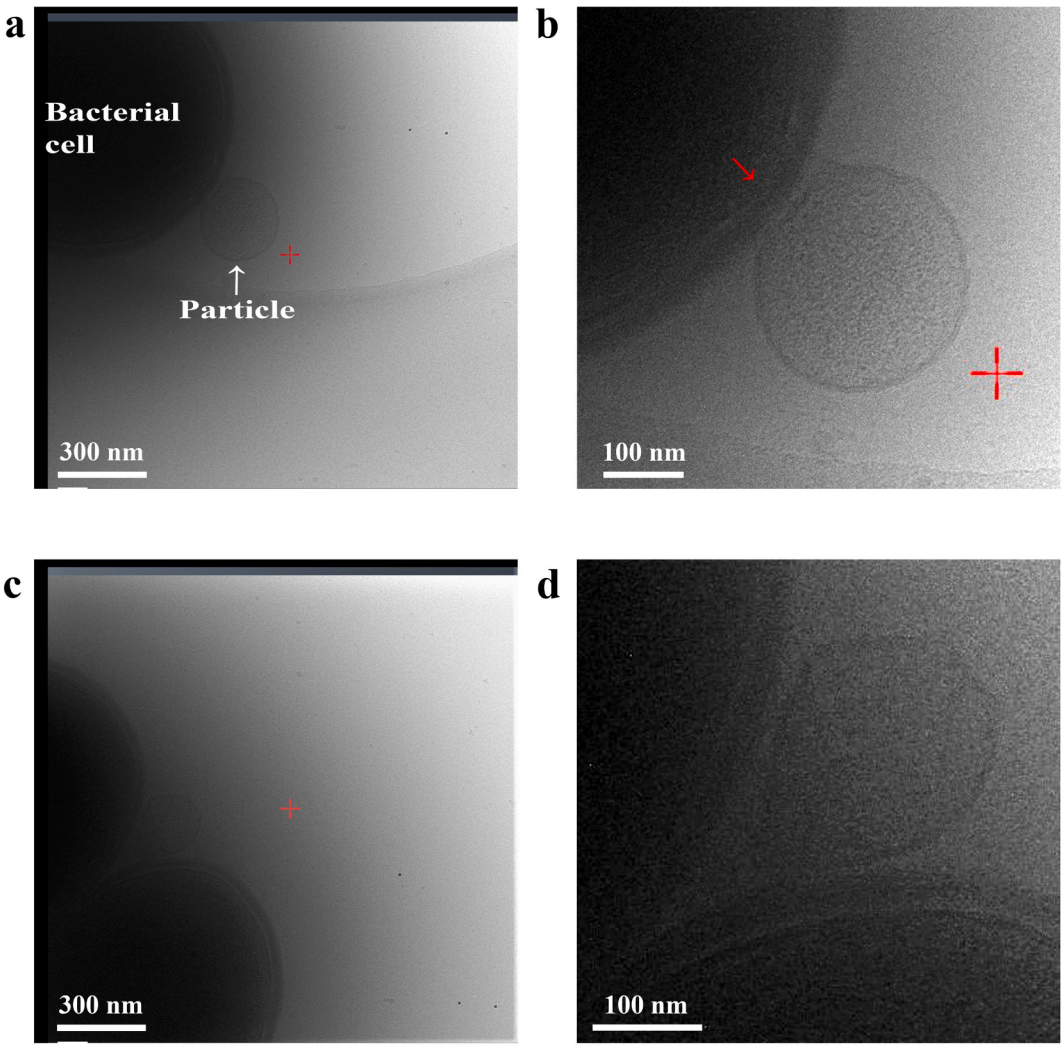

Fig. 10. Cryo-EM images taken of a solution of *S. aureus* that have been cultivated for 1 h together with antimicrobial particles. The brightness has been adjusted in the images for better clarity. (b) is a zoomed in image of (a), and (d) is a zoomed in image of (c). The red arrow indicates a section where potential membrane distortion appears (the red cross is a burned-in graphic, please disregard this). (For interpretation of the references to color in this figure legend, the reader is referred to the web version of this article.)

of reasons may contribute to the absence of secondary peaks obtained from the materials, namely low sensitivity of the SAXS instrument and in-situ drying of the materials during measurements, leading to higher probability of random scattering. This makes it difficult to determine the LLC phase from the diffractogram, but prior research on the LLCs of Pluronic F-127 at concentrations used to make the cross-linked hydrogels (30 wt% Pluronic F-127 and 70 wt% water) have been shown to be in the micellar cubic phase. The phase of the LLCs has also been shown in earlier studies to be maintained for a cross-linked system (He et al., 2015). Moreover, since we saw that the appearance of the diffractogram was maintained from the freshly cross-linked hydrogels to the freeze-dried particles, it can be deducted that the LLC phase found in the particles is maintained, meaning that they also have a micellar cubic structure. The slight peak shift to a higher q-value seen in the swollen particles indicates smaller spacing between structures. The reason behind this could be that the micelles swell up by taking up water, which makes them bigger, but since they are cross-linked to the other micelles in the cubic structure, they will not move further away from each other. This could result in the spacing between them becoming effectively smaller, explaining the q-shift.

The FTIR and Raman spectroscopy (Fig. 4 and Fig. 5) paint a clearer picture of what is going on in the particles during the manufacturing steps. For the pure DA-PF127 there were clear peaks indicating the vinyl group of the acrylate groups. The fact that they are not present for either of the freeze-dried particles indicates that the cross-linking by UV-polymerization has been successful. This is also clear from the fact that the hydrogel in Fig. 1d appears as a solid like piece. Furthermore, in the Raman spectra, there are three new peaks that appeared in the antimicrobial particles that were not present in the control particles. The three peaks can also be backtracked to the AMP, confirming the presence of AMPs in this sample. In the FTIR spectra the difference between the antimicrobial particles and the control particles is seen with the presence of a broad peak around 1650 cm^{-1} for the antimicrobial particles. This corresponds to the amide bonds of the AMP. The fingerprint region 800–1500 cm^{-1} in the FTIR spectra correlate well to that of Pluronic F-127. There was a slight peak shift and broadening observed in the C═O area for control and antimicrobial particles (peak at roughly 1735 cm^{-1}) compared to the DA-PF127 (peak at roughly 1725 cm^{-1}). It is, however, not possible to claim exactly what has caused this shift. From the Raman spectra we know that the particles do not have the vinyl group of the acrylate in them, meaning that the conjugated ester goes to a non-conjugated ester. While non-conjugated esters are found at higher wavenumbers, so are carboxylic acids. It is therefore difficult to say how much, if any, of the contribution of peak shift and broadening is due to

potential carboxylic acids and how much is from non-conjugated ester bonds. Regarding the antimicrobial particles, the expected outcome from the EDC/NHS activation is another amide bond, which is most likely engulfed by the amide bond peak of the AMPs, making it difficult to study the desired covalent bond between AMP and particle. The very small percentage of the mass that is the ester groups makes it difficult to interpret changes, since the peaks of these are much smaller in comparison to the rest of the material. The same goes for the peaks attributed to the AMP in the AMP-particle combination. UV–vis measurements showed that roughly 3.3 wt% of the dry weight was AMPs. It is therefore not surprising that the peaks attributed to the AMPs in the AMP-particles of both the Raman and FTIR are almost engulfed by the Pluronic peaks. What we do know, however, is that the AMP in the AMP-functionalized sample is present together with the LLC particles, since the samples that were evaluated with FTIR and Raman is completely void of water. Furthermore, from the UV–vis study we know that the particles took up roughly 3.3 times more AMP per gram compared to the hydrogel sheets. This indicates that the reaction is driven by the available surface more than available material. This supports the theory of covalent attachment of carboxylic acids found on the surfaces of the material with the amines found on the AMPs. Furthermore, the lack of any zone of inhibition around the antimicrobial particles in the agar plate model (Fig. 8) indicates that AMPs did not leach out from the particles. If the AMPs would have just been physically loaded into the particles, a clear zone around them due to leaching would have been excepted, and the lack of a zone further supports that the covalent attachment was successful.

The cytotoxicity and hemolysis results from Fig. 6 and Fig. 7 did not cause any concern for adverse effects. Even though the incorporation of AMPs to the particles did reduce the viability slightly compared to the control particles, the cell viability for the antibacterial particles were above the accepted as per ISO 10993 threshold of 70 % viability. For the hemolysis, the free AMPs showed that there is a concentration sweet spot for antibacterial effectiveness and danger to mammalian cells. In the range between 50 and 200 μM there is a significant hemolytic effect, and even 12.5 μM almost reached 20 % hemolysis. When the AMPs were covalently attached to the particles however, hemolysis was low for all concentrations tested. What is interesting here is that a concentration corresponding to higher than 200 μM AMP (which almost reached 100 % hemolysis in free state) is found at 12.5 mg/ml of antimicrobial particles, and these did not even reach 10 % hemolysis. This indicates that the AMPs might be less dangerous to mammalian cells when coupled to a material, even at higher concentrations.

The *in vitro* bacterial assays clearly showed an antibacterial effect by the antimicrobial particles. From the measured MIC values, the free AMP has a strong antibacterial effect against *S. aureus*, *S. epidermidis* and *E. coli* and also two MRSA strains. Unsurprisingly, a higher concentration was necessary in order to stop the growth of *P. aeruginosa,* which is known to be difficult to kill, but the concentration needed of the pure AMP was still quite low. By calculating the amount of AMP that was present in the antimicrobial particles, it was clear that 10–30 times more AMP was necessary to achieve bacterial growth inhibition compared to the free AMP. This is not too surprising, since the degree of freedom of the AMPs has been significantly reduced by physically locking them to the particle surface. It is important to keep in mind that the smallest particles (<6 μm) have been filtered out in the preparation steps, meaning that the particles with the highest mobility were not present. For *S. aureus*, *S. epidermidis, E. coli* and the two MRSA strains the MIC was still very low, indicating a strong antibacterial effect against theses strains. A much higher MIC was seen for *P. aeruginosa* and at up towards 25 mg of dry particles/ml the solution is starting to become more of a slurry, which is not suitable for all applications. For applications within wound care however, there are benefits in using a thicker slurry, similar to an ointment or cream. This form was tested in the agar plate model as shown in Fig. 8. From Fig. 8 there was a major antibacterial effect found against *S. aureus*, as a 4 log difference was observed between the antimicrobial particles and the control particles. Such a significant reduction of bacterial load could be essential for supporting wound healing after a trauma where infection is probable. The reason behind bacterial presence in the AMP-functionalized samples could be that the bacteria need to come in contact with the material in order to exert the antibacterial effect. This means that any gap in the particle coverage will provide a space for the bacterial growth. Translated to a potential wound, the conditions are not as good as on the agar plate and bacterial growth is slower. The reduction in bioburden determined for the antimicrobial particles should potentially assist the leukocytes in the wound healing, and hence lowering the risk of infection.

A strong motivation behind the attachment of the AMPs to the particles is to give them protection against serum. To investigate whether this holds true for the particles, a serum stability test was performed where the antibacterial activity against *S. epidermidis* was evaluated for free AMP and antimicrobial particles at two different concentrations. It was clear from the run without serum present that the free AMPs were much more efficient at killing the bacteria at the short timeframe of 10 min compared to the antimicrobial particles, and at much lower concentrations. With serum present, however, the antibacterial effect of the free AMPs was greatly reduced and after incubating together with serum for 1 day, all antibacterial effect was lost for the free AMPs. The antimicrobial particles, on the other hand, showed a lower antibacterial effect without serum present, but almost maintained all antibacterial effect even after 2 days of incubation with serum. This indicates strongly that the particles did indeed provide some protection of the AMPs towards the inhibition and degradation by the presence of serum. It should be noted that the particles did contain more AMPs per ml of solution compared to the free AMPs, similar to the MIC experiments. Although this is the absolute value of AMPs and the availability of AMPs on the surface of the particles are unknown. Increasing the free AMP concentration further might also lead to toxic behavior, as observed by the hemolysis study.

Interactions between the antimicrobial particles and the bacteria was investigated with cryo-EM. Particles of a size range matching the bigger peak of the DLS in Fig. 2 (~250 nm) were found in direct contact with bacteria. From Fig. 10b and Fig. 10d, a clear distortion of the particles was observed where the particles appear to be distorted along the surface of the bacteria. This indicates that there was an attraction between the bacterial cell wall and the particles. This attraction is probably an effect of the positively charged antimicrobial particles adhering to the negatively charged bacteria cell wall. In Fig. 10b it also appears that there is a thinning or some kind of distortion of the membrane/cell wall of the bacteria (marked with a red arrow) in proximity of the particle, indicating that the antimicrobial particle does have an effect on the structural integrity of the bacteria. There was, however, an evident issue with the bacteria of choice, *S. aureus*. The bigger size of the bacteria (~1 μm) resulted in a thicker ice being built up around them. This is the reason for the low clarity of the pictures around the bacteria. It was therefore not possible to see if any of the smaller particles (i.e. 20–60 nm as measured with the DLS) was present close to the bacteria, though they were observed elsewhere in the samples. It would be of great interest to analyze the interaction with smaller bacteria (e.g. mini-*E. coli*), which should result in sharper images as the ice would be much thinner around the cells. Potential interaction between the particles and the membrane should be determined in such a case. Furthermore, it would be beneficial to increase the concentration of the particles to improve the probability of finding particles and possible interactions with bacteria where the interaction could be studied in detail. The images presented are, however, representative of the interactions found.

This study has investigated hydrogel particles synthesized by crosslinking diacrylated PF-127 into sheets while in its micellar cubic lyotropic liquid crystal phase. The sheets were then mechanically reduced to particles, which in turn were made antibacterial by the covalently attachment of antimicrobial peptides to them. The particles showed antibacterial effect against a range of different bacterial strains including the antibiotic resistance strain MRSA. The attachment of the

AMPs provided them with protection from serum, as they retained their antibacterial effect, while free AMP did not. The attachment also reduced the hemolytic properties of the AMPs. Cryo-EM gave a glimpse into a potential antibacterial mechanism. To study the antimicrobial particles further, it would be of interest to try to take advantage of the lyotropic liquid crystals maintained in the particles and load the hydrophobic regions with a hydrophobic drug to see if a dual effect can be achieved. Obtaining different narrow size ranges of the particles would also be of great interest to investigate if a specific size has higher antibacterial effect or if a combination of sizes works better. This also goes hand in hand with closer studying interactions with the body in terms of uptake, degradation, and antibacterial effect *in vivo*.

5. Conclusions

The findings presented in this study have shown the development of antimicrobial particles made out of cross-linked lyotropic liquid crystals self-assembled from a block copolymer system with covalently bonded antimicrobial peptides. The LLC particles had a broad size distribution, with a major population in the range of 90 nm–30 μm. This resulted in a material that showed no cytotoxicity or hemolysis effect, but at the same time showed a good antibacterial effect against the gram-positive bacteria *S. aureus, S. epidermidis* as well as two MRSA strains and also the gram-negative bacteria *E. coli* and to a lower extent against the more resilient strain *P. aeruginosa*. An improved stability against serum was achieved by covalently attaching the AMPs to the particles, as the antimicrobial particles retained more of the antibacterial activity against *S. epidermidis* compared to free AMPs. Further insight was obtained from cryo-EM on the antibacterial mode-of-action of the LLC particles, whereby the antimicrobial particles seemed to closely interact with the membrane of the bacteria and potentially disrupt the same. In summary, the developed material poses a good base for an effective treatment or prevention of bacterial infections.

CRediT authorship contribution statement

Edvin Blomstrand: Methodology, Investigation, Visualization, Writing – original draft. **Anand K. Rajasekharan:** Supervision, Writing – review & editing. **Saba Atefyekta:** Project administration, Writing – review & editing. **Martin Andersson:** Conceptualization, Writing - review & editing.

Declaration of Competing Interest

The authors declare that they have no known competing financial interests or personal relationships that could have appeared to influence the work reported in this paper.

Data availability

Data will be made available on request.

Acknowledgements

The authors thank Camilla Holmlund at Umeå core facility for electron microscopy (Umeå University, Sweden) for assistance with cryogenic electron microscopy imaging, Chalmers Materials Analysis Laboratory (CMAL) for assistance with Fourier transform infra-red and Raman spectroscopy, and Jenny Perez Holmberg at Applied Chemistry, Chalmers University of Technology for assistance with DLS measurements. MA would like to thank the Knut And Alice Wallenberg Foundation through their Wallenberg Academy Fellow program and the Area of Advance for Materials Science at Chalmers University of Technology for funding.

Appendix A. Supplementary material

Supplementary data to this article can be found online at https://doi.org/10.1016/j.ijpharm.2022.122215.

References

Angelov, B., Angelova, A., Garamus, V.M., Drechsler, M., Willumeit, R., Mutafchieva, R., Štěpánek, P., Lesieur, S., 2012. Earliest stage of the tetrahedral nanochannel formation in cubosome particles from unilamellar nanovesicles. Langmuir 28 (48), 16647–16655.

Atefyekta, S., et al., 2019. Antibiofilm elastin-like polypeptide coatings: functionality, stability, and selectivity. Acta Biomater. 83, 245–256.

Atefyekta, S., Blomstrand, E., Rajasekharan, A.K., Svensson, S., Trobos, M., Hong, J., Webster, T.J., Thomsen, P., Andersson, M., 2021. Antimicrobial peptide-functionalized mesoporous hydrogels. ACS Biomater. Sci. Eng. 7 (4), 1693–1702.

Boge, L., Hallstensson, K., Ringstad, L., Johansson, J., Andersson, T., Davoudi, M., Larsson, P.T., Mahlapuu, M., Håkansson, J., Andersson, M., 2019. Cubosomes for topical delivery of the antimicrobial peptide LL-37. Eur. J. Pharm. Biopharm. 134, 60–67.

Chambers, H.F., DeLeo, F.R., 2009. Waves of resistance: *Staphylococcus aureus* in the antibiotic era. Nat. Rev. Microbiol. 7 (9), 629–641.

Chen, X., Schluesener, H.J., 2008. Nanosilver: a nanoproduct in medical application. Toxicol. Lett. 176 (1), 1–12.

Diniz, I.M.A., Chen, C., Xu, X., Ansari, S., Zadeh, H.H., Marques, M.M., Shi, S., Moshaverinia, A., 2015. Pluronic F-127 hydrogel as a promising scaffold for encapsulation of dental-derived mesenchymal stem cells. J. Mater. Sci. - Mater. Med. 26 (3) https://doi.org/10.1007/s10856-015-5493-4.

Gómez-Caravaca, A.M., Gómez-Romero, M., Arráez-Román, D., Segura-Carretero, A., Fernández-Gutiérrez, A., 2006. Advances in the analysis of phenolic compounds in products derived from bees. J. Pharm. Biomed. Anal. 41 (4), 1220–1234.

Håkansson, J., Cavanagh, J.P., Stensen, W., Mortensen, B., Svendsen, J.-S., Svenson, J., 2021. In vitro and in vivo antibacterial properties of peptide AMC-109 impregnated wound dressings and gels. J. Antibiot. 74 (5), 337–345.

He, W.-X., Rajasekharan, A.K., Tehrani-Bagha, A.R., Andersson, M., 2015. Mesoscopically ordered bone-mimetic nanocomposites. Adv. Mater. 27 (13), 2260–2264.

Holmqvist, P., Alexandridis, P., Lindman, B., 1997. Phase behavior and structure of ternary amphiphilic block copolymer– alkanol– water systems: comparison of poly (ethylene oxide)/poly (propylene oxide) to poly (ethylene oxide)/poly (tetrahydrofuran) copolymers. Langmuir 13 (9), 2471–2479.

Holmqvist, P., Alexandridis, P., Lindman, B., 1997. Modification of the microstructure in poloxamer block copolymer– water–"oil" systems by varying the "oil" type. Macromolecules 30 (22), 6788–6797.

Jain, J., Arora, S., Rajwade, J.M., Omray, P., Khandelwal, S., Paknikar, K.M., 2009. Silver nanoparticles in therapeutics: development of an antimicrobial gel formulation for topical use. Mol. Pharm. 6 (5), 1388–1401.

Kędziora, A., Speruda, M., Krzyżewska, E., Rybka, J., Łukowiak, A., Bugla-Płoskońska, G., 2018. Similarities and differences between silver ions and silver in nanoforms as antibacterial agents. Int. J. Mol. Sci. 19 (2), 444. https://doi.org/10.3390/ijms19020444.

Kim, H., Jang, J.H., Kim, S.C., Cho, J.H., 2014. De novo generation of short antimicrobial peptides with enhanced stability and cell specificity. J. Antimicrob. Chemother. 69 (1), 121–132.

Koehler, J., Brandl, F.P., Goepferich, A.M., 2018. Hydrogel wound dressings for bioactive treatment of acute and chronic wounds. Eur. Polym. J. 100, 1–11.

Krishnan, P.D., Banas, D., Durai, R.D., Kabanov, D., Hosnedlova, B., Kepinska, M., Fernandez, C., Ruttkay-Nedecky, B., Nguyen, H.V., Farid, A., Sochor, J., Narayanan, V.H.B., Kizek, R., 2020. Silver nanomaterials for wound dressing applications. Pharmaceutics 12 (9), 821. https://doi.org/10.3390/pharmaceutics12090821.

Kumarasamy, K.K., Toleman, M.A., Walsh, T.R., Bagaria, J., Butt, F., Balakrishnan, R., Chaudhary, U., Doumith, M., Giske, C.G., Irfan, S., Krishnan, P., Kumar, A.V., Maharjan, S., Mushtaq, S., Noorie, T., Paterson, D.L., Pearson, A., Perry, C., Pike, R., Rao, B., Ray, U., Sarma, J.B., Sharma, M., Sheridan, E., Thirunarayan, M.A., Turton, J., Upadhyay, S., Warner, M., Welfare, W., Livermore, D.M., Woodford, N., 2010. Emergence of a new antibiotic resistance mechanism in India, Pakistan, and the UK: a molecular, biological, and epidemiological study. Lancet. Infect. Dis 10 (9), 597–602.

Levy, S.B., Marshall, B., 2004. Antibacterial resistance worldwide: causes, challenges and responses. Nat. Med. 10 (S12), S122–S129.

Lim, K., Chua, R.R.Y., Ho, B., Tambyah, P.A., Hadinoto, K., Leong, S.S.J., 2015. Development of a catheter functionalized by a polydopamine peptide coating with antimicrobial and antibiofilm properties. Acta Biomater. 15, 127–138.

Magill, S.S., Edwards, J.R., Bamberg, W., Beldavs, Z.G., Dumyati, G., Kainer, M.A., Lynfield, R., Maloney, M., McAllister-Hollod, L., Nadle, J., Ray, S.M., Thompson, D. L., Wilson, L.E., Fridkin, S.K., 2014. Multistate point-prevalence survey of health care–associated infections. N. Engl. J. Med. 370 (13), 1198–1208.

Malmsten, M., et al., 2011. Highly selective end-tagged antimicrobial peptides derived from PRELP. PLoS ONE, 6(1), e16400.

Meikle, T.G., Dharmadana, D., Hoffmann, S.V., Jones, N.C., Drummond, C.J., Conn, C.E., 2021. Analysis of the structure, loading and activity of six antimicrobial peptides encapsulated in cubic phase lipid nanoparticles. J. Colloid Interface Sci. 587, 90–100.

Morones, J.R., Elechiguerra, J.L., Camacho, A., Holt, K., Kouri, J.B., Ramírez, J.T., Yacaman, M.J., 2005. The bactericidal effect of silver nanoparticles. Nanotechnology 16 (10), 2346–2353.
Müller, M., Becher, J., Schnabelrauch, M., Zenobi-Wong, M., 2015. Nanostructured pluronic hydrogels as bioinks for 3D bioprinting. Biofabrication 7 (3), 035006. https://doi.org/10.1088/1758-5090/7/3/035006.
Muller, M., Merrett, N.D., 2014. Pyocyanin production by Pseudomonas aeruginosa confers resistance to ionic silver. Antimicrob. Agents Chemother. 58 (9), 5492–5499.
Muszanska, A.K., Rochford, E.T.J., Gruszka, A., Bastian, A.A., Busscher, H.J., Norde, W., van der Mei, H.C., Herrmann, A., 2014. Antiadhesive polymer brush coating functionalized with antimicrobial and RGD peptides to reduce biofilm formation and enhance tissue integration. Biomacromolecules 15 (6), 2019–2026.
Neopane, P., et al., 2018. In vitro biofilm formation by *Staphylococcus aureus* isolated from wounds of hospital-admitted patients and their association with antimicrobial resistance. Int. J. Gen. Med. 11, 25.
Nguyen, L.T., et al., 2010. Serum stabilities of short tryptophan-and arginine-rich antimicrobial peptide analogs. PLoS ONE, 5(9), e12684.
Ong, S.-Y., Wu, J., Moochhala, S.M., Tan, M.-H., Lu, J., 2008. Development of a chitosan-based wound dressing with improved hemostatic and antimicrobial properties. Biomaterials 29 (32), 4323–4332.
Osei Sekyere, J., 2016. Current state of resistance to antibiotics of last-resort in South Africa: a review from a public health perspective. Front. Public Health 4, 209.
Pragatheeswaran, A.M., Chen, S.B., 2013. Effect of chain length of PEO on the gelation and micellization of the pluronic F127 copolymer aqueous system. Langmuir 29 (31), 9694–9701.
Selsted, M.E., Harwig, S.S., Ganz, T., Schilling, J.W., Lehrer, R.I., 1985. Primary structures of three human neutrophil defensins. J. Clin. Investig. 76 (4), 1436–1439.
Shai, Y., 2002. Mode of action of membrane active antimicrobial peptides. Peptide Sci.: Original Res. Biomol. 66 (4), 236–248.
Su, Y., Wang, H., Mishra, B., Lakshmaiah Narayana, J., Jiang, J., Reilly, D.A., Hollins, R. R., Carlson, M.A., Wang, G., Xie, J., 2019. Nanofiber dressings topically delivering molecularly engineered human cathelicidin peptides for the treatment of biofilms in chronic wounds. Mol. Pharm. 16 (5), 2011–2020.
Wang, N., et al., 2020. Nisin-loaded polydopamine/hydroxyapatite composites: biomimetic synthesis, and in vitro bioactivity and antibacterial activity evaluations. Colloids Surf. A: Physicochem. Eng. Aspects, 125101.
Wang, Y., Beekman, J., Hew, J., Jackson, S., Issler-Fisher, A.C., Parungao, R., Lajevardi, S.S., Li, Z., Maitz, P.K.M., 2018. Burn injury: challenges and advances in burn wound healing, infection, pain and scarring. Adv. Drug Deliv. Rev. 123, 3–17.
Yasin, B., Pang, M., Turner, J.S., Cho, Y., Dinh, N.-N., Waring, A.J., Lehrer, R.I., Wagar, E.A., 2000. Evaluation of the inactivation of infectious Herpes simplex virus by host-defense peptides. Eur. J. Clin. Microbiol. Infect. Dis. 19 (3), 187–194.
Zasloff, M., 2002. Antimicrobial peptides of multicellular organisms. Nature 415 (6870), 389–395.
Zerkoune, L., Lesieur, S., Putaux, J.-L., Choisnard, L., Gèze, A., Wouessidjewe, D., Angelov, B., Vebert-Nardin, C., Doutch, J., Angelova, A., 2016. Mesoporous self-assembled nanoparticles of biotransesterified cyclodextrins and nonlamellar lipids as carriers of water-insoluble substances. Soft Matter 12 (36), 7539–7550.
Zhu, J., Han, H., Li, F., Wang, X., Yu, J., Qin, X., Wu, D., 2019. Peptide-functionalized amino acid-derived pseudoprotein-based hydrogel with hemorrhage control and antibacterial activity for wound healing. Chem. Mater. 31 (12), 4436–4450.
Zhu, G., Zhu, X., Fan, Q.i., Wan, X., 2011. Raman spectra of amino acids and their aqueous solutions. Spectrochim. Acta Part A Mol. Biomol. Spectrosc. 78 (3), 1187–1195.
Zuarez-Easton, S., et al., 2017. Postcesarean wound infection: prevalence, impact, prevention, and management challenges. Int. J Women's Health 9, 81.